Spin-Wave Doppler Shift by Magnon Drag in Magnetic Insulators

Tao Yu,[1] Chen Wang,[2] Michael A. Sentef,[1] and Gerrit E. W. Bauer[3]
[1]Max Planck Institute for the Structure and Dynamics of Matter, Luruper Chaussee 149, 22761 Hamburg, Germany
[2]Center for Joint Quantum Studies and Department of Physics, School of Science, Tianjin University, Tianjin 300350, China
[3]WPI-AIMR and Institute for Materials Research and CSRN, Tohoku University, Sendai 980-8577, Japan

(Received 30 November 2020; accepted 5 March 2021; published 30 March 2021)

The Doppler shift of the quasiparticle dispersion by charge currents is responsible for the critical supercurrents in superconductors and instabilities of the magnetic ground state of metallic ferromagnets. Here we predict an analogous effect in thin films of magnetic insulators in which microwaves emitted by a proximity stripline generate coherent chiral spin currents that cause a Doppler shift in the magnon dispersion. The spin-wave instability is suppressed by magnon-magnon interactions that limit spin currents to values close to but below the threshold for the instability. The spin current limitations by the backaction of magnon currents on the magnetic order should be considered as design parameters in magnonic devices.

DOI: 10.1103/PhysRevLett.126.137202

Introduction.—Realization of a large spin current is an important pursuit in spintronics. Electrically insulating magnetic films are promising candidates to achieve this goal, allowing low-dissipation information processing by magnons [1–5]. The presently most suitable material to study magnon dynamics is yttrium iron garnet (YIG), a ferrimagnet with high Curie temperature and arguably the lowest damping [6,7]. Ultrathin YIG films with thicknesses below 10 nm maintain very high magnetic quality [8,9] and a strongly enhanced Drude-type magnon conductivity [10–12] that should be suitable to carry large spin currents. Recently, large spin currents were observed in ultrathin YIG transistors with dc-current-biased Pt gates that inject a large number of nonequilibrium magnons [13–16] into the conducting channel [11,17].

A Doppler shift of Bogoliubov quasiparticles under an electric current bias is responsible for critical supercurrents in superconductors [18–20]. A similar effect can happen in metallic ferromagnets when using electric currents to excite magnetization dynamics by the spin-transfer torque 21,22]]. The charge current induces a Doppler shift, i.e., a tilt of the spin-wave dispersion of a homogeneous magnetization in momentum space, which could trigger a spin-wave instability [23–25] and modulate the magnetic ground state [26]. These obviously do not apply to magnetic insulators that cannot carry an electric charge current. However, magnetic insulators are also conduits for (magnonic) spin currents that, as reported here, cause a nonlinear Doppler effect by magnon-magnon drag, which also limit the spin current to a material-dependent maximum.

In this Letter, we formulate the dynamics of long-wavelength coherent magnons of thin YIG films in the presence of large magnon currents that are pumped by stripline microwaves as depicted in Fig. 1. The polarization-momentum-locked ac magnetic field emitted by a microwave stripline [27–29] coherently populates magnon states at one side of the stripline with a unidirectional magnon current. We report here that (i) magnon interactions limit the magnitude of this magnon current and the chirality of the pumping, and (ii) an interaction-induced drag effect by the spin current on the magnon dynamics in the form of a magnonic Doppler shift tilts the spin-wave dispersion into the current direction. The physics of the reported Doppler effect differs strongly from the magnon drag by phonon [30] or electron [23–25,31] currents.

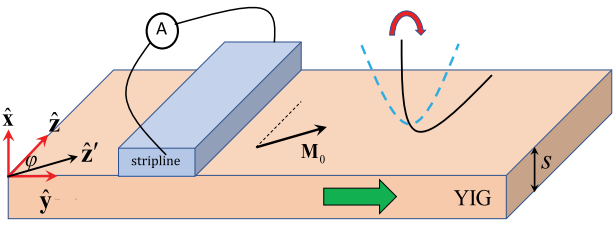

FIG. 1. Doppler effect of thin magnetic films driven by pure magnon current. A long stripline along the $\hat{\mathbf{z}}$ direction is illustrated to pump the magnon current (the green thick arrow) in YIG films of thickness s that causes the tilt of magnon dispersion, as shown by the red thick arrow and parabolic bands. The in plane magnetization is saturated with a relative angle φ to the stripline direction.

Its phenomenology is intriguingly similar to an interfacial Dzyaloshinskii-Moriya interaction (DMI) [32–34], but can be tuned by the excitation power. Interaction renders a linear (rather than quadratic) dependence of the excited spin current amplitude at small driving currents. When the drive currents reach a critical value, the Doppler shift leads to a dispersion in which the magnon energy vanishes for a finite momentum state, which corresponds to an instability of the ferromagnetic order. However, for stronger drives, higher-order magnon interactions stabilize the magnetization ground state and suppress the spin-wave instability by breaking the chirality of chiral pumping. We thereby predict a maximum spin current that is close to but (in the absence of a DMI assist) not large enough to cause a spin-wave instability.

Maximal spin current.—We consider an in plane magnetized YIG film with thickness $s = \mathcal{O}(10)$ nm and saturated magnetization M_s, with surface normal oriented along the $\hat{\mathbf{x}}$ direction. An in plane static magnetic field $\mathbf{H}_{\rm app}$ is applied at an angle φ to the stripline $\hat{\mathbf{z}}$ direction (Fig. 1). The Hamiltonian of the magnetic order reads

$$\hat{H} = \mu_0 \int \left(\frac{\alpha_{\rm ex}}{2} (\nabla \hat{\mathbf{M}})^2 - \hat{\mathbf{M}} \cdot \mathbf{H}_{\rm app} \right) d\mathbf{r}, \tag{1}$$

where μ_0 is the vacuum permeability, $\alpha_{\rm ex}$ is the exchange stiffness, and $\mathbf{M}$ is the magnetization. We disregard anisotropies [35,36] because the crystal ones are small in YIG, while the dipolar ones are strongly suppressed in the thin film limit [37,38]. The exchange length in YIG is $\lambda_{\rm ex} = 2\pi\sqrt{\alpha_{\rm ex}} = 109$ nm since $\alpha_{\rm ex} = 3 \times 10^{-16}$ m^2 [39,40]. The magnetization dynamics then obeys a Landau-Lifshitz-Gilbert (LLG) equation

$$\frac{d\mathbf{M}}{dt} = -\mu_0 \gamma \mathbf{M} \times (\mathbf{H}_{\rm app} + \alpha_{\rm ex} \nabla^2 \mathbf{M}) + \frac{\alpha_{\rm G}}{M_s} \mathbf{M} \times \frac{d\mathbf{M}}{dt}, \tag{2}$$

where α_G is the Gilbert damping constant and $-\gamma$ is the electron gyromagnetic ratio. In the absence of external torques and damping, the magnetization carries a magnetization current density

$$\tilde{\mathbf{j}}_\delta = \alpha_{\rm ex} \mu_0 \gamma \mathbf{M} \times \nabla_\delta \mathbf{M}, \tag{3}$$

which satisfies the continuity equation $d\mathbf{M}/dt + \nabla \cdot \tilde{\mathbf{j}} = 0$ [41]. When considering the excitation of magnetization, we include the microwave field $\mathbf{H}(t)$ in the LLG equation.

The microwaves emitted by a long stripline on top of a thin magnetic film launch a coherent magnon current normal to it. We consider a metallic wire of rectangular cross section $0 < x < d$ and $-w/2 < y < w/2$ (Fig. 1) with an ac current density I of frequency ω_s. The microwaves are uniform over the film thickness when $s \ll d$. The Fourier component k_y of the Oersted magnetic field in the thin film below the stripline ($x \to -s/2$) reads [27–29,42–44]

$$\begin{aligned} H_x(k_y, \omega_s) &= (i/2) I(\omega_s) \mathcal{F}(d, w) \mathrm{sgn}(k_y) e^{-|k_y|(d+s)/2}, \\ H_y(k_y, \omega_s) &= -(1/2) I(\omega_s) \mathcal{F}(d, w) e^{-|k_y|(d+s)/2}, \end{aligned} \tag{4}$$

with $\mathcal{F}(d, w) = (2/k_y^2) \sin(k_y w/2)(1 - e^{-|k_y|d})$ determined by stripline dimensions. Here we used $|k_y| \gg \omega_s/c$ because the velocity of light c is much larger than that of the magnons. The magnetic field $H_y(k_y, \omega_s) = i\mathrm{sgn}(k_y) H_x(k_y, \omega_s)$ is right and left circularly polarized for positive and negative k_y, respectively, so polarization and momentum are locked. In the linear regime, this field coherently excites circularly polarized magnons that propagate unidirectionally and populate at one side of the stripline, i.e., a chiral pumping effect. This picture will be thoroughly changed in the nonlinear regime, however (see below).

Figure 2 illustrates the pumped magnon spin current $\mathbf{J}_y(y=0) = -1/(2\omega_M \gamma \alpha_{\rm ex}) \int_{-s}^{0} dx \tilde{\mathbf{j}}_y(x, y=0)$ with $\omega_M \equiv \mu_0 \gamma M_s$ as a function of the applied electric current density I with frequency $\omega_s \approx \{5.8, 11.3\}$ GHz across the stripline of width $w = \{150, 200\}$ nm and thickness $d = 80$ nm [8,44] from numerical solutions of the LLG equation. Here the YIG film thickness $s = 10$ nm, the applied static magnetic field $\mu_0 H_{\rm app} = 10$ mT that drives out domain walls [8,40], $\mu_0 M_s = 0.18$ T, and $\alpha_G = 10^{-4}$. With the increase of the biased current in the stripline, the spin currents first linearly increase but become saturated or maximal at a critical electric current I_c. This phenomenon is completely unexpected for noninteracting magnons that should scale as $|\mathbf{J}_y| \propto I^2$, which highlights the importance of the interaction effects discussed in the following.

Magnonic Doppler effect.—The LLG phenomenology contains all of the nonlinearities that can be captured by interacting magnons to some extent. The Holstein-Primakoff transformation expresses the magnetization dynamics by bosonic magnon operators $\hat{\Theta}(\mathbf{r})$ with $\hat{S}_x(\mathbf{r}) + i\hat{S}_{y'}(\mathbf{r}) = \hat{\Theta}^\dagger(\mathbf{r}) \sqrt{2S - \hat{\Theta}^\dagger(\mathbf{r}) \hat{\Theta}(\mathbf{r})}$ and

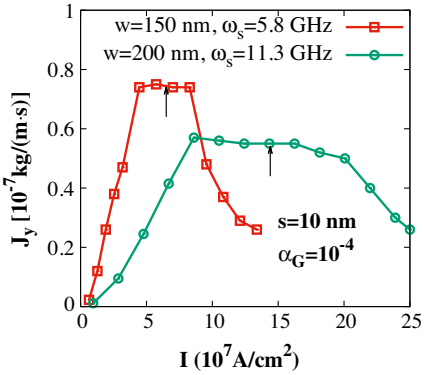

FIG. 2. Maximum spin current excited in a magnetic film with thickness $s = 10$ nm by an ac charge current density I in a proximity microwave stripline calculated by numerically solving the LLG equation. The black arrows indicate the critical current density I_c for the indicated frequencies ω_s and stripline widths w.

$\hat{S}_{z'}(\mathbf{r}) = -S + \hat{\Theta}^\dagger(\mathbf{r})\hat{\Theta}(\mathbf{r})$, where the spin operators $\hat{\mathbf{S}} = -\mathbf{M}/(\gamma\hbar)$. The leading terms in the expansion of the square roots leads to a complete set of harmonic oscillators that we use to expand the full problem. The eigenmodes normal to the film plane depend on the boundary conditions that become free for thin films [45]. The magnon operators in position space can then be expanded in perpendicular standing spin waves (PSSWs) with index l [37,38]

$$\hat{\Theta}(\mathbf{r}) = \sum_{l\geq 0} \sqrt{\frac{2}{1+\delta_{l0}}} \frac{1}{\sqrt{s}} \cos\left(\frac{l\pi}{s}x\right) \hat{\Psi}_l(\boldsymbol{\rho}), \tag{5}$$

where $\boldsymbol{\rho} = y\hat{\mathbf{y}} + z\hat{\mathbf{z}}$. Substituting these expressions into the Holstein-Primakoff expansion, the Hamiltonian can be written as $\hat{H} = \hat{H}_L + \hat{H}_{\rm NL} + \cdots$, where $\hat{H}_L$ describes the noninteracting magnon gas and $\hat{H}_{\rm NL}$ is the leading nonlinear term that introduces interactions between the magnons. At sufficiently low magnon densities

$$\hat{H} \to \hat{H}_L = \sum_l (E_l + \hbar\omega_M \alpha_{\rm ex} k^2) \int \hat{\Psi}_l^\dagger(\boldsymbol{\rho}) \hat{\Psi}_l(\boldsymbol{\rho}) d\boldsymbol{\rho}, \tag{6}$$

where $E_l = \mu_0\gamma\hbar H_{\rm app} + \hbar\omega_M\alpha_{\rm ex}(l\pi/s)^2$ is the edge of the lth band. The nonlinear Hamiltonian

$$\hat{H}_{\rm NL} = \sum_{l_i} \mathcal{U}_{l_1l_2l_3l_4} \int \hat{\Psi}^\dagger_{l_1}(\boldsymbol{\rho})\hat{\Psi}^\dagger_{l_2}(\boldsymbol{\rho})\hat{\Psi}_{l_3}(\boldsymbol{\rho})\hat{\Psi}_{l_4}(\boldsymbol{\rho}) d\boldsymbol{\rho} + \sum_{l_i} \mathcal{V}_{l_1l_2l_3l_4} \int \hat{\Psi}^\dagger_{l_1}(\boldsymbol{\rho})\hat{\Psi}^\dagger_{l_2}(\boldsymbol{\rho}) \nabla_{\boldsymbol{\rho}}\hat{\Psi}_{l_3} \cdot \nabla_{\boldsymbol{\rho}}\hat{\Psi}_{l_4} d\boldsymbol{\rho} + \text{H.c.}$$

contains two types of magnon-number conserving interactions derived in the Supplemental Material [46]. The potentials

$$\mathcal{U}_{l_1l_2l_3l_4} = \frac{\mu_0\gamma^2\hbar^2\alpha_{\rm ex} l_3 l_4 \pi^2 \mathcal{A}_{l_1l_2l_3l_4}}{s^3\sqrt{(1+\delta_{l_10})(1+\delta_{l_20})(1+\delta_{l_30})(1+\delta_{l_40})}},$$
$$\mathcal{V}_{l_1l_2l_3l_4} = \frac{\mu_0\gamma^2\hbar^2\alpha_{\rm ex} \mathcal{B}_{l_1l_2l_3l_4}}{s\sqrt{(1+\delta_{l_10})(1+\delta_{l_20})(1+\delta_{l_30})(1+\delta_{l_40})}}$$

are governed by magnon-mode overlap integrals

$$\mathcal{A}_{l_1l_2l_3l_4} = \frac{1}{s}\int_{-s}^{0} dx \Pi_{i=1,2} \cos\left(\frac{l_i\pi}{s}x\right) \Pi_{j=3,4} \sin\left(\frac{l_j\pi}{s}x\right),$$
$$\mathcal{B}_{l_1l_2l_3l_4} = \frac{1}{s}\int_{-s}^{0} dx \Pi_{i=1,2,3,4} \cos\left(\frac{l_i\pi}{s}x\right).$$

When $l_1 = 0$, the scattering potentials obey selection rules $\mathcal{U}_{0l_2l_3l_4} \propto l_3 l_4(\delta_{l_2+l_3,l_4} + \delta_{l_2+l_4,l_3} - \delta_{l_3+l_4,l_2})$ and $\mathcal{V}_{0l_2l_3l_4} \propto (\delta_{l_2+l_3,l_4} + \delta_{l_2+l_4,l_3} + \delta_{l_2+l_3+l_4,0} + \delta_{l_3+l_4,l_2})$. In the two-dimensional limit, $\mathcal{U}_{0000} = 0$ vanishes, but $\mathcal{V}_{0000} = \mathcal{V}_{00ll} = \mathcal{V}_0 = \mu_0\gamma^2\hbar^2\alpha_{\rm ex}/(4s)$ is large. The divergence for vanishing film thickness is an artifact of the continuum approximation that breaks down when s approaches unit cell dimensions.

We are interested in the effect of a magnon current on a low-frequency coherent excitation, i.e., at excitation frequency $\omega/(2\pi) \lesssim 1$ GHz, which allows us to set $l_1 = 0$. Using the above selection rules of the scattering potentials and energy conservation, we prove in the Supplemental Material [46] that the incoherent scattering of these *low-energy* magnons by those in all other bands is marginally small. The leading nonlinearities in the coherent magnon states thus reduce to a self-consistent mean-field problem [47,48], in which the interaction renormalizes the energy dispersion but does not affect magnon dephasing and lifetime. The coherent magnon amplitude in the lowest band obeys a Heisenberg equation of motion that is augmented by the Gilbert damping [46],

$$i\hbar(1 - i\alpha_G)\frac{\partial\langle\hat{\Psi}_0(\boldsymbol{\rho})\rangle}{\partial t} = E_0\langle\hat{\Psi}_0(\boldsymbol{\rho})\rangle - \hbar\omega_M\alpha_{\rm ex}\nabla^2\langle\hat{\Psi}_0(\boldsymbol{\rho})\rangle + \frac{8i}{\hbar}\sum_{l'\geq 0}\mathcal{V}_{00l'l'}\mathbf{J}_{l'}(\boldsymbol{\rho})\cdot\nabla_{\boldsymbol{\rho}}\langle\hat{\Psi}_0(\boldsymbol{\rho})\rangle + P_{\rm ex}, \tag{7}$$

where $\langle\cdots\rangle$ represents an ensemble average,

$$\mathbf{J}_l(\boldsymbol{\rho}) = \frac{\hbar}{2i}(\langle\hat{\Psi}^\dagger_l(\boldsymbol{\rho})\nabla_{\boldsymbol{\rho}}\hat{\Psi}_l(\boldsymbol{\rho})\rangle - \langle\hat{\Psi}_l(\boldsymbol{\rho})\nabla_{\boldsymbol{\rho}}\hat{\Psi}^\dagger_l(\boldsymbol{\rho})\rangle) \tag{8}$$

is the magnon linear-momentum current density in subband l with contributions from both coherent and incoherent magnons, and $P_{\rm ex}$ is a microwaves excitation source that will be specified below. The (locally) uniform magnon current hence engages the gradient (or momentum) of the magnon amplitude $\nabla_{\boldsymbol{\rho}}\langle\hat{\Psi}_0\rangle$ and tilts the magnon dispersion, which is an interaction-induced drag effect [30,31].

The magnon momentum current density [Eq. (8)] is proportional to the magnon-number current density $\tilde{\mathbf{J}}_l$ defined by the continuity and Heisenberg equations for the noninteracting magnon Hamiltonian, since the exchange magnons have a constant mass $\hbar/(2\omega_M\alpha_{\rm ex})$. The former is also a spin current since, in the absence of anisotropies, the magnons carry angular momentum $\hbar$. With magnon density operator $\hat{\rho}^l_m(\boldsymbol{\rho}) = \langle\hat{\Psi}^\dagger_l(\boldsymbol{\rho})\hat{\Psi}_l(\boldsymbol{\rho})\rangle$,

$$\frac{\partial\hat{\rho}^l_m(\boldsymbol{\rho})}{\partial t} = \frac{1}{i\hbar}[\hat{\rho}^l_m(\boldsymbol{\rho}), \hat{H}_L] = -\nabla\cdot\tilde{\mathbf{J}}_l(\boldsymbol{\rho}), \tag{9}$$

leading to $\langle\tilde{\mathbf{J}}_l(\boldsymbol{\rho})\rangle = (2\omega_M\alpha_{\rm ex}/\hbar)\mathbf{J}_l(\boldsymbol{\rho})$, which is consistent with Eq. (3) since $-1/(\gamma\hbar)\int dx\tilde{\mathbf{j}}(x,\boldsymbol{\rho}) \to \tilde{\mathbf{J}}_l(\boldsymbol{\rho})$ when $l = 0$ to linear order in the magnon operator.

This stripline microwave field [Eq. (4)] couples to the magnons of the lowest PSSW band up to wave numbers $k_y \sim \pi/w$ by the Zeeman interaction

$$\hat{H}_Z = g\sum_{k_y}[H_x(k_y,t) - i\cos\varphi H_y(k_y,t)]\hat{\Psi}_0^\dagger(k_y) + \text{H.c.},$$

with coupling constant $g = \mu_0\sqrt{\gamma\hbar M_s s/2}$, so the excitation source $P_{\rm ex} = g[H_x(k_y,t) - i\cos\varphi H_y(k_y,t)]$ in Eq. (7). The in plane magnetization angle φ can be rotated by an applied dc magnetic field to tune the magnitude and direction of the pumped magnon current. When $\varphi = 0$, the stripline magnetic field launches a magnon current with $k_y > 0$ into half space (see below). Thereby, the excited magnon current $\mathbf{J}_y(y>0) = \bar{\mathbf{J}}_y \exp(-y/\delta)$ decays exponentially with distance from the source on the scale of the decay length $\delta(\omega_s) \sim 2/\mathrm{Im}\kappa_y \sim \sqrt{(\alpha_{\rm ex}\omega_M)(\omega_s - \mu_0\gamma H_{\rm app})}/(\alpha_G\omega_s)$, i.e., the root of $(\omega_s - \mu_0\gamma H_{\rm app} - \omega_M\alpha_{\rm ex}\kappa_y^2)^2 + (\alpha_G\omega_s)^2 = 0$. On the other hand, the amplitude $\langle\hat{\Psi}_0(\boldsymbol{\rho})\rangle$ oscillates rapidly with wavelength $(1/|\kappa_y| \ll \delta)$. Near the stripline, the magnon current in the lowest band obeys the integral equation, obtained from Eq. (7),

$$\bar{\mathbf{J}}_y = \frac{1}{\delta}\left(\frac{g}{\hbar}\right)^2 \int \frac{dk_y}{2\pi} k_y \frac{|H_x(k_y) - iH_y(k_y)|^2}{(\omega_s - \tilde{\omega}_{k_y})^2 + \alpha_G^2\omega_s^2}, \quad (10)$$

with Doppler-shifted magnon frequency

$$\tilde{\omega}_{\mathbf{k}} = \mu_0\gamma H_{\rm app} + \omega_M\alpha_{\rm ex}k^2 - (8/\hbar^2)\mathcal{V}_0 k_y \bar{\mathbf{J}}_y, \quad (11)$$

which can be solved iteratively or graphically.

Figure 3(a) illustrates the pumped magnon current $\bar{\mathbf{J}}_y$ as a function of the applied electric current density I with frequency $\omega_s/(2\pi) \approx 0.93$ GHz across the stripline of width $w = 150$ nm and thickness $d = 80$ nm [8,44] from Eq. (10), in comparison with numerical solutions of the LLG equation [Eq. (3)]. Magnons of wavelength $2w$ are resonantly excited and carry a current with decay length $\delta \approx 333$ μm. Here we compare the analytical solutions with the numerically exact solution of the LLG equation, which predicts a maximum spin-wave current for a stripline current $I_c \approx 5\times10^7$ A/cm^2. The noninteracting spin-wave theory (SW free) fails already for small I, which emphasizes the importance of nonlinearities. When including the drag effect, the spin-wave theory (10) $\bar{\mathbf{J}}_y$ saturates at a current $I \sim I_c$, but returns to the noninteracting values at larger currents. When $I > I_c$, the lowest-order nonlinearity of the Holstein-Primakoff expansion and thereby the mean-field theory may break down. The Doppler shift of the spin-wave dispersion illustrated in Fig. 3(b) holds only for $I < I_c$. More detailed comparison with different parameters confirms these features [46]. When $I \gtrsim I_c$, we observe that the chirality of the magnon excitation is strongly reduced, indicating that the backscattering of magnons becomes strong, as illustrated by Figs. 4(c) and 4(d), which is partly responsible for the suppression of spin current.

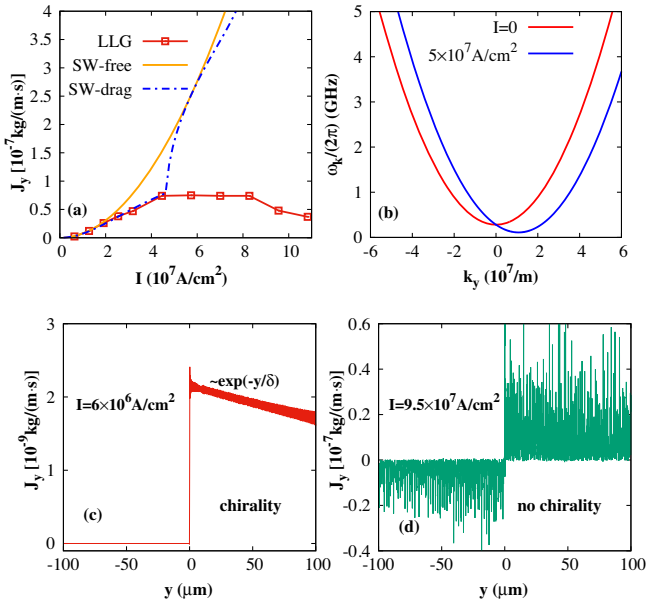

FIG. 3. Magnon currents and Doppler shift of the magnon dispersion under stripline microwave excitation. (a) The coherently pumped magnon current $\bar{\mathbf{J}}_y$ as a function of the applied electric current density I in the stripline from numerical LLG calculations ("LLG"), noninteracting spin-wave theory ("SW-free"), and spin-wave theory including the drag effect ("SW-drag"). The tilt of the magnon dispersion at high excitation is illustrated in (b). We illustrate the chirality of the spin-current excitation for $I < I_c$ (c) and $I > I_c$ (d), respectively.

I_c can be estimated by the onset of a spin-wave instability that is characterized by negative magnon excitation energy [23,24,26], which causes the discontinuous change of the spin current calculated by the mean-field theory. According to Eq. (11), a critical magnon current

$$\mathbf{J}_y^{(c)} = \hbar/(4\mathcal{V}_0)\sqrt{\hbar\omega_M\alpha_{\rm ex}E_0} \quad (12)$$

can cause negative magnon excitation energies $\tilde{E}_0(\mathbf{k}) < 0$ at the momentum $k_y^{(c)} = 4\mathcal{V}_0\bar{\mathbf{J}}_y/(\hbar^2\omega_M\alpha_{\rm ex})$. With the above YIG parameters, the critical magnon current $\mathbf{J}_y^{(c)} \approx 10^{-7}$ kg/(m s). This value can be reached by incoherent spin injection with a critical temperature gradient 4 K/μm when $T = 300$ K [46]. However, according to the LLG calculations in Fig. 2, with different material parameters nonlinearities might prohibit reaching this critical value, which thus provides an upper limit in the estimation of maximal spin currents (more detailed comparison in the Supplemental Material [46]).

The tilt of dispersion causes chiral velocities of spin waves of the same energy that should be observable by changes in the microwave transmission [8,40], nitrogen-vacancy center magnetometry [44,49], and Brillouin light scattering [50]. The dispersion tilts into the opposite

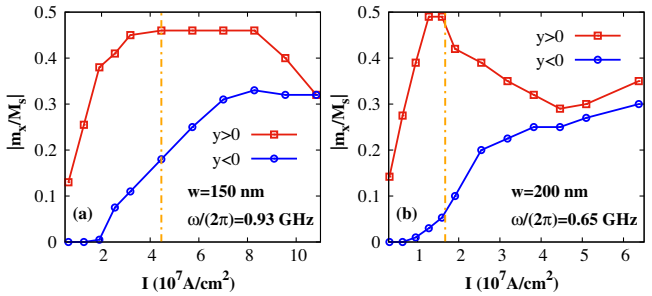

FIG. 4. Magnon densities (reduced magnetization) at the right and left side of a stripline as a function of current density I with (a) $\omega_s = 2\pi \times 0.93$ GHz and width $w = 150$ nm, and (b) $2\pi \times 0.65$ GHz and width $w = 200$ nm. The vertical orange line indicates the critical I_c that maximizes the spin current.

direction when the magnetization direction is reversed ($\varphi = \pi$) and vanishes when perpendicular to the stripline ($\varphi = \pi/2$); i.e., it follows the current direction governed by the chirality of the stripline magnetic field. The basic features agree with recently reported experiments in YIG thin films of thickness $s = 7$ nm [8] that were interpreted in terms of the DMI, although spin-orbit interaction is small for closed-shell magnetic moments [51]. The Doppler effect, on the other hand, is tunable by the magnitude and direction of the excited magnonic spin current and does not require special interfaces. We note that an interfacial DMI causes additional shift of the magnon dispersion that favors the realization of spin-wave instability as calculated in the Supplemental Material [46].

Breaking of chiral pumping.—Finally, mean-field theory reveals a connection between the breakdown of the chiral pumping and the spin-wave instability. Around the critical driving strength I_c, the magnon density on one side of the stripline reaches its maximum with a rapid increase of the magnon density on the other side. Figure 4 shows the suppression of chirality under strong excitation. The nonequilibrium magnetization for $y > 0$ is largest around I_c, at which magnons accumulate also at $y < 0$. The chirality is strongly broken for larger drives, with nearly equal excited magnon densities on both sides of the stripline such that the injected power propagates into both directions, similar to the electric or thermal injection of an incoherent magnon accumulation.

Discussion.—In conclusion, we formulated the dynamics of a strongly driven ultrathin film of magnetic insulator such as YIG. We predict a Doppler shift of the magnon dispersion and a maximum spin current that a given sample can sustain. In our example, the effects should occur at stripline current densities $\sim 2 \times 10^7$ A/cm^2 in one or $\sim (2/\mathcal{N}) \times 10^7$ A/cm^2 in $\mathcal{N}$ striplines (distributed over a total width that should be small compared to the magnon propagation length, i.e., many micrometers). The nonmonotonic dependence of the spin current excited by microwave power may be related to the observed nonmonotonicity of spin transport in magnon transistors as a function of gate-injected magnon densities [11,17]. Our theory should help in understanding the effects of large magnon spin currents on the magnetic order of insulators and provides a different scenario for the nonlinearities induced by the magnon chemical potential [13–16,52–55].

This work is financially supported by DFG Emmy Noether program (SE 2558/2-1) as well as JSPS KAKENHI Grant No. 19H006450. C. W. is supported by the National Natural Science Foundation of China under Grant No. 11704061. We thank Xiang-Yang Wei, Hanchen Wang, Haiming Yu, and Mehrdad Elyasi for valuable discussions.

[1] B. Lenk, H. Ulrichs, F. Garbs, and M. Muenzenberg, Phys. Rep. **507**, 107 (2011).
[2] A. V. Chumak, V. I. Vasyuchka, A. A. Serga, and B. Hillebrands, Nat. Phys. **11**, 453 (2015).
[3] D. Grundler, Nat. Nanotechnol. **11**, 407 (2016).
[4] V. E. Demidov, S. Urazhdin, G. de Loubens, O. Klein, V. Cros, A. Anane, and S. O. Demokritov, Phys. Rep. **673**, 1 (2017).
[5] A. Brataas, B. van Wees, O. Klein, G. de Loubens, and M. Viret, Phys. Rep. **885**, 1 (2020).
[6] H. Chang, P. Li, W. Zhang, T. Liu, A. Hoffmann, L. Deng, and M. Wu, IEEE Magn. Lett. **5**, 6700104 (2014).
[7] V. Cherepanov, I. Kolokolov, and V. L'vov, Phys. Rep. **229**, 81 (1993).
[8] H. C. Wang, J. L. Chen, T. Liu, J. Y. Zhang, K. Baumgaertl, C. Y. Guo, Y. H. Li, C. P. Liu, P. Che, S. Tu, S. Liu, P. Gao, X. F. Han, D. P. Yu, M. Z. Wu, D. Grundler, and H. M. Yu, Phys. Rev. Lett. **124**, 027203 (2020).
[9] J. Mendil, M. Trassin, Q. Bu, J. Schaab, M. Baumgartner, C. Murer, P. T. Dao, J. Vijayakumar, D. Bracher, C. Bouillet, C. A. F. Vaz, M. Fiebig, and P. Gambardella, Phys. Rev. Mater. **3**, 034403 (2019).
[10] L. J. Cornelissen, J. Liu, B. J. van Wees, and R. A. Duine, Phys. Rev. Lett. **120**, 097702 (2018).
[11] T. Wimmer, M. Althammer, L. Liensberger, N. Vlietstra, S. Geprägs, M. Weiler, R. Gross, and H. Huebl, Phys. Rev. Lett. **123**, 257201 (2019).
[12] L. J. Cornelissen, K. J. H. Peters, G. E. W. Bauer, R. A. Duine, and B. J. van Wees, Phys. Rev. B **94**, 014412 (2016).
[13] P. W. Anderson and H. Suhl, Phys. Rev. **100**, 1788 (1955).
[14] V. S. L'vov, *Wave Turbulence Under Parametric Excitation* (Springer-Verlag, Berlin, Heidelberg, 1994).
[15] S. O. Demokritov, V. E. Demidov, G. A. Melkov, A. A. Serga, B. Hillebrands, and A. N. Slavin, Nature (London) **443**, 430 (2006).
[16] J. Liu, F. Feringa, B. Flebus, L. J. Cornelissen, J. C. Leutenantsmeyer, R. A. Duine, and B. J. van Wees, Phys. Rev. B **99**, 054420 (2019).
[17] J. Liu, X.-Y. Wei, G. E. W. Bauer, J. Ben Youssef, and B. J. van Wees, arXiv:2011.07800.
[18] P. Fulde, *Tunneling Phenomena in Solids* (Plenum, New York, 1969).

[19] A. Kohen, Th. Proslier, T. Cren, Y. Noat, W. Sacks, H. Berger, and D. Roditchev, Phys. Rev. Lett. **97**, 027001 (2006).
[20] T. Yu and M. W. Wu, Phys. Rev. B **94**, 205305 (2016).
[21] S. Zhang and Z. Li, Phys. Rev. Lett. **93**, 127204 (2004).
[22] Y. Tserkovnyak, H. J. Skadsem, A. Brataas, and G. E. W. Bauer, Phys. Rev. B **74**, 144405 (2006).
[23] Ya. B. Bazaliy, B. A. Jones, and S.-C. Zhang, Phys. Rev. B **57**, R3213(R) (1998).
[24] J. Fernández-Rossier, M. Braun, A. S. Núñez, and A. H. MacDonald, Phys. Rev. B **69**, 174412 (2004).
[25] R. J. Doornenbal, A. Roldán-Molina, A. S. Nunez, and R. A. Duine, Phys. Rev. Lett. **122**, 037203 (2019).
[26] J. Shibata, G. Tatara, and H. Kohno, Phys. Rev. Lett. **94**, 076601 (2005).
[27] T. Schneider, A. A. Serga, T. Neumann, B. Hillebrands, and M. P. Kostylev, Phys. Rev. B **77**, 214411 (2008).
[28] V. E. Demidov, M. P. Kostylev, K. Rott, P. Krzysteczko, G. Reiss, and S. O. Demokritov, Appl. Phys. Lett. **95**, 112509 (2009).
[29] T. Yu and G. E. W. Bauer, in *Chirality, Magnetism, and Magnetoelectricity: Separate Phenomena and Joint Effects in Metamaterial Structures*, edited by E. Kamenetskii (Springer International Publishing, New York, 2021).
[30] A. V. Chumak, P. Dhagat, A. Jander, A. A. Serga, and B. Hillebrands, Phys. Rev. B **81**, 140404(R) (2010).
[31] V. Vlaminck and M. Bailleul, Science **322**, 410 (2008).
[32] I. A. Dzyaloshinsky, J. Phys. Chem. Solids **4**, 241 (1958).
[33] T. Moriya, Phys. Rev. Lett. **4**, 228 (1960).
[34] J.-H. Moon, S.-M. Seo, K.-J. Lee, K.-W. Kim, J. Ryu, H.-W. Lee, R. D. McMichael, and M. D. Stiles, Phys. Rev. B **88**, 184404 (2013).
[35] T. Wolfram and R. E. De Wames, Phys. Rev. Lett. **24**, 1489 (1970).
[36] B. A. Kalinikos, M. P. Kostylev, N. V. Kozhus, and A. N. Slavin, J. Phys. Condens. Matter **2**, 9861 (1990).
[37] C. Bayer, J. Jorzick, B. Hillebrands, S. O. Demokritov, R. Kouba, R. Bozinoski, A. N. Slavin, K. Y. Guslienko, D. V. Berkov, N. L. Gorn, and M. P. Kostylev, Phys. Rev. B **72**, 064427 (2005).
[38] T. Yu, C. P. Liu, H. M. Yu, Y. M. Blanter, and G. E. W. Bauer, Phys. Rev. B **99**, 134424 (2019).
[39] S. Klingler, A. V. Chumak, T. Mewes, B. Khodadadi, C.Mewes, C. Dubs, O. Surzhenko, B. Hillebrands, and A. Conca, J. Phys. D **48**, 015001 (2015).
[40] H. C. Wang, J. L. Chen, T. Yu, C. P. Liu, C. Y. Guo, H. Jia, S. Liu, K. Shen, T. Liu, J. Y. Zhang, M. A. Cabero Z, Q. M. Song, S. Tu, L. Flacke, M. Althammer, M. Weiler, M. Z. Wu, X. F. Han, K. Xia, D. P. Yu, G. E. W. Bauer, and H. M. Yu, arXiv:2005.10452.
[41] Y. Tserkovnyak and M. Kläui, Phys. Rev. Lett. **119**, 187705 (2017).
[42] J. D. Jackson, *Classical Electrodynamics* (Wiley, New York, 1998).
[43] P. Lodahl, S. Mahmoodian, S. Stobbe, A. Rauschenbeutel, P. Schneeweiss, J. Volz, H. Pichler, and P. Zoller, Nature (London) **541**, 473 (2017).
[44] I. Bertelli, J. J. Carmiggelt, T. Yu, B. G. Simon, C. C. Pothoven, G. E. W. Bauer, Y. M. Blanter, J. Aarts, and T. van der Sar, Sci. Adv. **6**, eabd3556 (2020).
[45] Q. Wang, B. Heinz, R. Verba, M. Kewenig, P. Pirro, M. Schneider, T. Meyer, B. Lagel, C. Dubs, T. Bracher, and A. V. Chumak, Phys. Rev. Lett. **122**, 247202 (2019).
[46] See Supplemental Material at http://link.aps.org/supplemental/10.1103/PhysRevLett.126.137202 for the derivation of interaction Hamiltonian and incoherent exchange scattering, detailed comparison of spin currents with different parameters, and discussion of the effects of interfacial DMI.
[47] A. A. Abrikosov, L. P. Gorkov, and I. E. Dzyaloshinski, *Methods of Quantum Field Theory in Statistical Physics* (Prentice Hall, Englewood Cliffs, NJ, 1963).
[48] A. Griffin, T. Nikuni, and E. Zaremba, *Bose-Condensed Gases at Finite Temperatures* (Cambridge University Press, Cambridge, England, 2009).
[49] F. Casola, T. van der Sar, and A. Yacoby, Nat. Rev. Mater. **3**, 17088 (2018).
[50] S. O. Demokritov, B. Hillebrands, and A. N. Slavin, Phys. Rep. **348**, 441 (2001).
[51] L. Caretta, E. Rosenberg, F. Bütner, T. Fakhrul, P. Gargiani, M. Valvidares, Z. Chen, P. Reddy, D. A. Muller, C. A. Ross, and G. S. D. Beach, Nat. Commun. **11**, 1090 (2020).
[52] S. A. Bender, R. A. Duine, A. Brataas, and Y. Tserkovnyak, Phys. Rev. B **90**, 094409 (2014).
[53] B. Flebus, S. A. Bender, Y. Tserkovnyak, and R. A. Duine, Phys. Rev. Lett. **116**, 117201 (2016).
[54] C. Du, T. V. der Sar, T. X. Zhou, P. Upadhyaya, F. Casola, H. Zhang, M. C. Onbasli, C. A. Ross, R. L. Walsworth, Y. Tserkovnyak, and A. Yacoby, Science **357**, 195 (2017).
[55] C. Ulloa, A. Tomadin, J. Shan, M. Polini, B. J. van Wees, and R. A. Duine, Phys. Rev. Lett. **123**, 117203 (2019).

Spin-Wave Doppler Shift by Magnon Drag in Magnetic Insulators: Supplemental Material

Tao Yu,[1] Chen Wang,[2] Michael A. Sentef,[1] and Gerrit E. W. Bauer[3]

[1] *Max Planck Institute for the Structure and Dynamics of Matter, Luruper Chaussee 149, 22761 Hamburg, Germany*

[2] *Center for Joint Quantum Studies and Department of Physics, School of Science, Tianjin University, Tianjin 300350, China*

[3] *Institute for Materials Research and WPI-AIMR and CSRN, Tohoku University, Sendai 980-8577, Japan*

(Dated: February 9, 2021)

I. NONLINEAR HAMILTONIAN

We consider an in-plane magnetized YIG film with surface normal along the $\hat{\mathbf{x}}$-direction and a static magnetic field $\mathbf{H}_{\rm app}$ applied along the $\hat{\mathbf{z}}'$-direction (see Fig. 1 in the main text). We adopt the following Hamiltonian for the YIG film magnetization

$$\hat{H} = \mu_0 \int \left[\frac{\alpha_{\rm ex}}{2} \left(\nabla \hat{\mathbf{M}} \right)^2 - \hat{\mathbf{M}} \cdot \frac{\hat{\mathbf{H}}_{\rm dip}}{2} - \hat{\mathbf{M}} \cdot \mathbf{H}_{\rm app} \right] d\mathbf{r}, \tag{S1}$$

where μ_0 is the vacuum permeability, $\alpha_{\rm ex}$ is the exchange stiffness, and $\mathbf{H}_{\rm dip}$ is the dipolar field. We recover the spin operators by the replacement $\hat{\mathbf{M}} = -\gamma\hbar\hat{\mathbf{S}}$ with $-\gamma$ being the electron gyromagnetic ratio, leading to

$$\hat{H} = \mu_0 \int \left[\frac{\gamma\hbar}{2} \mathbf{S}(\mathbf{r}) \cdot \hat{\mathbf{H}}_{\rm dip}(\mathbf{r}) + \frac{\gamma^2\hbar^2\alpha_{\rm ex}}{2} \nabla\mathbf{S} \cdot \nabla\mathbf{S} + \gamma\hbar\mathbf{S} \cdot \mathbf{H}_{\rm ext} \right] d\mathbf{r}. \tag{S2}$$

We may disregard the dipolar interaction in ultrathin magnetic films that are excited by narrow striplines. In terms of the magnon field operator $\hat{\Theta}(\mathbf{r})$, the Holstein-Primakoff transformation reads

$$\begin{aligned}
&\hat{S}_x(\mathbf{r}) + i\hat{S}_{y'}(\mathbf{r}) = \hat{\Theta}^\dagger(\mathbf{r}) \sqrt{2S - \hat{\Theta}^\dagger(\mathbf{r})\hat{\Theta}(\mathbf{r})}, \\
&\hat{S}_x(\mathbf{r}) - i\hat{S}_{y'}(\mathbf{r}) = \sqrt{2S - \hat{\Theta}^\dagger(\mathbf{r})\hat{\Theta}(\mathbf{r})}\hat{\Theta}(\mathbf{r}), \\
&\hat{S}_{z'}(\mathbf{r}) = -S + \hat{\Theta}^\dagger(\mathbf{r})\hat{\Theta}(\mathbf{r}).
\end{aligned} \tag{S3}$$

In a thin magnetic film wave interference leads to standing waves normal to the interfaces. Assuming free boundary conditions, the magnon operator can be expanded as

$$\hat{\Theta}(\mathbf{r}) = \sum_l \sqrt{\frac{2}{1+\delta_{l0}}} \frac{1}{\sqrt{s}} \cos\left(\frac{l\pi}{s} x \right) \hat{\Psi}_l(\boldsymbol{\rho}), \tag{S4}$$

where l is the subband index and s the film thickness. In terms of $\hat{\Psi}_l(\boldsymbol{\rho})$, the in-plane magnon field operators for subband l, the Zeeman Hamiltonian reads

$$\begin{aligned}
\hat{H}_{\rm Z} &= \mu_0\gamma\hbar \int \hat{S}_z H_{\rm app} d\mathbf{r} = \mu_0\gamma\hbar H_{\rm app} \int \hat{\Theta}^\dagger\hat{\Theta} d\mathbf{r} \\
&\to \mu_0\gamma\hbar H_{\rm app} \sum_l \int \hat{\Psi}_l^\dagger(\boldsymbol{\rho})\hat{\Psi}_l(\boldsymbol{\rho}) d\boldsymbol{\rho}.
\end{aligned} \tag{S5}$$

The linear exchange Hamiltonian

$$\begin{aligned}
\hat{H}_{\rm ex}^{\rm L} &= \mu_0\gamma\hbar M_s\alpha_{\rm ex} \int \nabla\hat{\Theta}^\dagger \cdot \nabla\hat{\Theta} d\mathbf{r} \\
&\to \mu_0\gamma\hbar M_s\alpha_{\rm ex} \sum_{l\geq 1} \left(\frac{l\pi}{s} \right)^2 \int \hat{\Psi}_l^\dagger(\boldsymbol{\rho})\hat{\Psi}_l(\boldsymbol{\rho}) d\boldsymbol{\rho} + \mu_0\gamma\hbar M_s\alpha_{\rm ex} \sum_l \int \nabla_{\boldsymbol{\rho}}\hat{\Psi}_l^\dagger(\boldsymbol{\rho}) \cdot \nabla_{\boldsymbol{\rho}}\hat{\Psi}_l(\boldsymbol{\rho}) d\boldsymbol{\rho}.
\end{aligned} \tag{S6}$$

The subbands edges of the magnon dispersion are therefore at

$$E_l = \mu_0\gamma\hbar H_{\rm app} + \mu_0\gamma\hbar M_s\alpha_{\rm ex}(l\pi/s)^2. \tag{S7}$$

In a YIG film with thickness below 10 nm and at temperatures $T \lesssim 300$ K, only the lowest three bands $l = \{0, 1, 2\}$ are significantly populated.

The leading non-linear exchange Hamiltonian is given by

$$\begin{aligned}\hat{H}_{\rm ex}^{\rm NL} &= \frac{\mu_0\gamma^2\hbar^2\alpha_{\rm ex}}{4}\int\left(\hat{\Theta}^\dagger(\mathbf{r})\hat{\Theta}^\dagger(\mathbf{r})\nabla\Theta\cdot\nabla\Theta+\text{H.c.}\right)d\mathbf{r}\\ &= \sum_{l_1l_2l_3l_4}\mathcal{U}_{l_1l_2l_3l_4}\int\hat{\Psi}^\dagger_{l_1}(\boldsymbol{\rho})\hat{\Psi}^\dagger_{l_2}(\boldsymbol{\rho})\hat{\Psi}_{l_3}(\boldsymbol{\rho})\hat{\Psi}_{l_4}(\boldsymbol{\rho})d\boldsymbol{\rho}\\ &+ \sum_{l_1l_2l_3l_4}\mathcal{V}_{l_1l_2l_3l_4}\int\hat{\Psi}^\dagger_{l_1}(\boldsymbol{\rho})\hat{\Psi}^\dagger_{l_2}(\boldsymbol{\rho})\nabla_{\boldsymbol{\rho}}\hat{\Psi}_{l_3}(\boldsymbol{\rho})\cdot\nabla_{\boldsymbol{\rho}}\hat{\Psi}_{l_4}(\boldsymbol{\rho})d\boldsymbol{\rho}+\text{H.c.},\end{aligned}\tag{S8}$$

in which

$$\begin{aligned}\mathcal{U}_{l_1l_2l_3l_4} &= \frac{\mu_0\gamma^2\hbar^2\alpha_{\rm ex}}{4s}\frac{4}{\sqrt{(1+\delta_{l_10})(1+\delta_{l_20})(1+\delta_{l_30})(1+\delta_{l_40})}}\frac{l_3\pi}{s}\frac{l_4\pi}{s}\mathcal{A}_{l_1l_2l_3l_4},\\ \mathcal{V}_{l_1l_2l_3l_4} &= \frac{\mu_0\gamma^2\hbar^2\alpha_{\rm ex}}{4s}\frac{4}{\sqrt{(1+\delta_{l_10})(1+\delta_{l_20})(1+\delta_{l_30})(1+\delta_{l_40})}}\mathcal{B}_{l_1l_2l_3l_4},\end{aligned}\tag{S9}$$

with form factors

$$\begin{aligned}\mathcal{A}_{l_1l_2l_3l_4} &= \frac{1}{s}\int_{-s}^{0}\cos\left(\frac{l_1\pi}{s}x\right)\cos\left(\frac{l_2\pi}{s}x\right)\sin\left(\frac{l_3\pi}{s}x\right)\sin\left(\frac{l_4\pi}{s}x\right)dx\\ &= \frac{1}{8}\left(\delta_{l_1+l_2+l_3,l_4}+\delta_{l_1+l_2+l_4,l_3}+\delta_{l_1+l_3,l_2+l_4}+\delta_{l_1+l_4,l_2+l_3}\right.\\ &\left.-\delta_{l_1+l_2+l_3+l_4,0}-\delta_{l_1+l_2,l_3+l_4}-\delta_{l_1+l_3+l_4,l_2}-\delta_{l_2+l_3+l_4,l_1}\right),\\ \mathcal{B}_{l_1l_2l_3l_4} &= \frac{1}{s}\int_{-s}^{0}\cos\left(\frac{l_1\pi}{s}x\right)\cos\left(\frac{l_2\pi}{s}x\right)\cos\left(\frac{l_3\pi}{s}x\right)\cos\left(\frac{l_4\pi}{s}x\right)dx\\ &= \frac{1}{8}\left(\delta_{l_1+l_2+l_3,l_4}+\delta_{l_1+l_2+l_4,l_3}+\delta_{l_1+l_3,l_2+l_4}+\delta_{l_1+l_4,l_2+l_3}+\delta_{l_1+l_2+l_3+l_4,0}\right.\\ &\left.+\delta_{l_1+l_2,l_3+l_4}+\delta_{l_1+l_3+l_4,l_2}+\delta_{l_2+l_3+l_4,l_1}\right).\end{aligned}\tag{S10}$$

The interaction strength increases with decreasing film thickness. Here we focus on the interaction of $\langle\hat{\Psi}_{l=0}(\boldsymbol{\rho})\rangle$, i.e. the coherent magnons in the lowest band $l_1=0$, and those in the thermally populated higher bands. $\mathcal{A}_{0l_2l_3l_4}$-processes with $\{l_3,l_4\}\neq 0$ are governed by the selection rules

$$\begin{aligned}\mathcal{A}_{0l_2l_3l_4} &= \frac{1}{4}\left(\delta_{l_2+l_3,l_4}+\delta_{l_2+l_4,l_3}-\delta_{l_3+l_4,l_2}\right),\\ \mathcal{B}_{0l_2l_3l_4} &= \frac{1}{4}\left(\delta_{l_2+l_3,l_4}+\delta_{l_2+l_4,l_3}+\delta_{l_2+l_3+l_4,0}+\delta_{l_3+l_4,l_2}\right).\end{aligned}\tag{S11}$$

With $[\hat{\Psi}_{l'}(\boldsymbol{\rho}'),\hat{\Psi}^\dagger_l(\boldsymbol{\rho})]=\delta_{ll'}\delta(\boldsymbol{\rho}-\boldsymbol{\rho}')$ and the Heisenberg equation $i\hbar\partial_t\hat{\Psi}_{l'}(\boldsymbol{\rho}')=[\hat{\Psi}_{l'}(\boldsymbol{\rho}'),\hat{H}]$, the dynamics of the coherent magnons in the lowest band ($l=0$) obeys

$$\begin{aligned}i\hbar\frac{\partial\langle\hat{\Psi}_{l=0}(\boldsymbol{\rho})\rangle}{\partial t} &= E_{l=0}\langle\hat{\Psi}_{l=0}(\boldsymbol{\rho})\rangle-\hbar\omega_M\alpha_{\rm ex}\nabla^2\langle\hat{\Psi}_{l=0}(\boldsymbol{\rho})\rangle\\ &+2\sum_{l_2l_3l_4}\mathcal{U}_{0l_2l_3l_4}\langle\hat{\Psi}^\dagger_{l_2}(\boldsymbol{\rho})\hat{\Psi}_{l_3}(\boldsymbol{\rho})\hat{\Psi}_{l_4}(\boldsymbol{\rho})\rangle+2\sum_{l_1l_2l_3}\mathcal{U}_{l_1l_2l_30}\langle\hat{\Psi}_{l_1}(\boldsymbol{\rho})\hat{\Psi}_{l_2}(\boldsymbol{\rho})\hat{\Psi}^\dagger_{l_3}(\boldsymbol{\rho})\rangle\\ &+2\sum_{l_2l_3l_4}\mathcal{V}_{0l_2l_3l_4}\left(\langle\hat{\Psi}^\dagger_{l_2}\nabla_{\boldsymbol{\rho}}\hat{\Psi}_{l_3}\cdot\nabla_{\boldsymbol{\rho}}\hat{\Psi}_{l_4}\rangle-\nabla_{\boldsymbol{\rho}}\cdot\langle\hat{\Psi}_{l_2}\hat{\Psi}_{l_3}\nabla_{\boldsymbol{\rho}}\hat{\Psi}^\dagger_{l_4}\rangle\right),\end{aligned}\tag{S12}$$

where $\omega_H=\mu_0\gamma H_{\rm app}$ and $\omega_M=\mu_0\gamma M_s$. The terms involving $\mathcal{U}$ vanish in the mean-field approximation of the 3-magnon amplitudes when $\langle\hat{\Psi}_{l\neq0}(\boldsymbol{\rho})\rangle=0$. The last term in Eq. (S12) when transformed into momentum

space reduces to

$$
\begin{aligned}
&-\frac{4}{\hbar}\sum_{\mathbf{k}}\sum_{l'}\mathcal{V}_{ll'l'}e^{i\mathbf{k}\cdot\boldsymbol{\rho}}\mathbf{k}\cdot\left(\sum_{\mathbf{k}'}\hbar\mathbf{k}'\left(\langle\hat{\Psi}_{l'}(\mathbf{k}')\hat{\Psi}^{\dagger}_{l'}(\mathbf{k}')\rangle+\langle\hat{\Psi}^{\dagger}_{l'}(\mathbf{k}')\hat{\Psi}_{l'}(\mathbf{k}')\rangle\right)\right)\langle\Psi_{l}(\mathbf{k})\rangle\\
&=\frac{8i}{\hbar}\sum_{l'}\mathcal{V}_{ll'l'}\nabla_{\boldsymbol{\rho}}\langle\hat{\Psi}_{l}(\boldsymbol{\rho})\rangle\cdot\frac{\hbar}{2i}\left(\langle\hat{\Psi}^{\dagger}_{l'}(\boldsymbol{\rho})\nabla_{\boldsymbol{\rho}}\hat{\Psi}_{l'}(\boldsymbol{\rho})\rangle-\langle\hat{\Psi}_{l'}(\boldsymbol{\rho})\nabla_{\boldsymbol{\rho}}\hat{\Psi}^{\dagger}_{l'}(\boldsymbol{\rho})\rangle\right).
\end{aligned}
\tag{S13}
$$

We recognize the magnon current density in subband l' (in units of an angular momentum current J/m^2)

$$
\mathbf{J}_{l'}(\boldsymbol{\rho})=\frac{\hbar}{2i}\left(\langle\hat{\Psi}^{\dagger}_{l'}(\boldsymbol{\rho})\nabla_{\boldsymbol{\rho}}\hat{\Psi}_{l'}(\boldsymbol{\rho})\rangle-\langle\hat{\Psi}_{l'}(\boldsymbol{\rho})\nabla_{\boldsymbol{\rho}}\hat{\Psi}^{\dagger}_{l'}(\boldsymbol{\rho})\rangle\right),
\tag{S14}
$$

which can be integrated to an expression in terms of magnon occupation numbers

$$
\boldsymbol{\mathcal{J}}_{l'}=\int\mathbf{J}_{l'}(\boldsymbol{\rho})d\boldsymbol{\rho}=\frac{1}{2}\sum_{\mathbf{k}'}\hbar\mathbf{k}'\left(\langle\hat{\Psi}^{\dagger}_{l'}(\mathbf{k}')\hat{\Psi}_{l'}(\mathbf{k}')\rangle+\langle\hat{\Psi}_{l'}(\mathbf{k}')\hat{\Psi}^{\dagger}_{l'}(\mathbf{k}')\rangle\right).
\tag{S15}
$$

$\mathbf{J}$ is a spin current since the magnons carry spin $\hbar$. The expressions are consistent with the magnon density current $\tilde{\mathbf{J}}_l$ defined by the Heisenberg equation and the magnon conservation law (in the absence of damping)

$$
\frac{\partial\hat{\rho}^{l}_{m}}{\partial t}=\frac{1}{i\hbar}[\hat{\rho}^{l}_{m},\hat{H}^{\mathrm{L}}_{\mathrm{ex}}]=-\nabla\cdot\tilde{\mathbf{J}}_{l},
\tag{S16}
$$

which leads to

$$
\left\langle\tilde{\mathbf{J}}_{l}(\boldsymbol{\rho})\right\rangle=\omega_{M}\alpha_{\mathrm{ex}}\frac{1}{i}\left(\langle\hat{\Psi}^{\dagger}_{l}(\boldsymbol{\rho})\nabla_{\boldsymbol{\rho}}\hat{\Psi}_{l}(\boldsymbol{\rho})\rangle-\langle\hat{\Psi}_{l}(\boldsymbol{\rho})\nabla_{\boldsymbol{\rho}}\hat{\Psi}^{\dagger}_{l}(\boldsymbol{\rho})\rangle\right),
\tag{S17}
$$

which equals $\mathbf{J}_l$ divided by the constant magnon mass. The coherent magnons in the lowest band thereby obey

$$
\begin{aligned}
i\hbar\frac{\partial\langle\hat{\Psi}_{0}(\boldsymbol{\rho})\rangle}{\partial t}&=E_{l=0}\langle\hat{\Psi}_{0}(\boldsymbol{\rho})\rangle-\hbar\omega_{M}\alpha_{\mathrm{ex}}\nabla^{2}\langle\hat{\Psi}_{0}(\boldsymbol{\rho})\rangle\\
&+\frac{8i}{\hbar}\sum_{l'}\mathcal{V}_{00l'l'}\nabla_{\boldsymbol{\rho}}\langle\hat{\Psi}_{0}(\boldsymbol{\rho})\rangle\cdot\mathbf{J}_{l'}(\boldsymbol{\rho}).
\end{aligned}
\tag{S18}
$$

Both incoherent and coherent magnons contribute to the current density $\mathbf{J}_{l'}$.

A magnon current carried by incoherent or thermal magnons can be driven by a magnon chemical potential or temperature gradients. These can be created either by the spin-Hall effect in, or Ohmic heating of, current-biased Pt contacts. We can estimate the latter (spin Seebeck) effect by the linearized Boltzmann equation in the relaxation-time approximation. Assuming that the drag term in the collision integral is small

$$
-\mathbf{v}_{\mathbf{k},l}\cdot\nabla T\frac{\partial f_{\mathbf{k},l}}{\partial T}=-\frac{f_{\mathbf{k},l}-f^{(0)}_{\mathbf{k},l}}{\tau_{\mathbf{k},l}},
\tag{S19}
$$

where $\mathbf{v}_{\mathbf{k},l}=(1/\hbar)\partial E_l(\mathbf{k})/\partial\mathbf{k}=2\omega_M\alpha_{\mathrm{ex}}\mathbf{k}$ is the magnon group velocity, $f_{\mathbf{k},l}=\langle\hat{\Psi}^{\dagger}_{l}(\mathbf{k})\hat{\Psi}_{l}(\mathbf{k})\rangle$ is the magnon distribution in the l-th subband, $f^{(0)}_{\mathbf{k},l}=1/\{\exp[E_{\mathbf{k},l}/(k_BT)]-1\}$ is the equilibrium Planck distribution at temperature T, and $\tau_{\mathbf{k},l}$ is the magnon relaxation time. A uniform $\nabla T=\mathcal{E}_y\hat{\mathbf{y}}$ then generates a magnon momentum current

$$
\mathbf{J}_{l}=\hbar\omega_{M}\alpha_{\mathrm{ex}}\mathcal{E}_{y}\hat{\mathbf{y}}\int\frac{dk_{y}dk_{z}}{2\pi^{2}}k_{y}^{2}\tau_{\mathbf{k},l}\frac{\partial f^{(0)}_{\mathbf{k},l}}{\partial T},
\tag{S20}
$$

which affects the coherent magnon amplitude by substitution into Eq. (S18).

To complete the dynamic equation, we need to account for the scattering between magnons which requires a treatment beyond the mean-field approximation, which we address in the next section.

II. ABSENCE OF EXCHANGE SCATTERING OF LOW-ENERGY MAGNONS

Here we describe the scattering processes between the coherent magnon of the lowest band and the incoherent thermal cloud by dividing the magnon operator of the lowest band into a coherent number amplitude Ξ and incoherent operator $\hat{\psi}$

$$\begin{aligned}\hat{\Psi}_0(\boldsymbol{\rho},t) &= \Xi(\boldsymbol{\rho},t) + \hat{\psi}_0(\boldsymbol{\rho},t) \approx \Xi(t) + \hat{\psi}_0(\boldsymbol{\rho},t),\\ \hat{\Psi}_{l>0}(\boldsymbol{\rho},t) &= \hat{\psi}_l(\boldsymbol{\rho},t).\end{aligned} \tag{S21}$$

The first interaction term

$$H_{\rm int}^{(1)} \to 2\sum_{l_2 l_3 l_4} \mathcal{U}_{0 l_2 l_3 l_4} \Xi^*(t) \int \hat{\psi}_{l_2}^\dagger(\boldsymbol{\rho}) \hat{\psi}_{l_3}(\boldsymbol{\rho}) \hat{\psi}_{l_4}(\boldsymbol{\rho}) d\boldsymbol{\rho} + \text{H.c.}, \tag{S22}$$

with selection rules $\delta_{l_2+l_3,l_4}$, $\delta_{l_2+l_4,l_3}$, and $\delta_{l_3+l_4,l_2}$; the second interaction term

$$\hat{H}_{\rm int}^{(2)} \to 2\sum_{l_2 l_3 l_4} \mathcal{V}_{0 l_2 l_3 l_4} \Xi^*(t) \int \hat{\psi}_{l_2}^\dagger(\boldsymbol{\rho}) \nabla_{\boldsymbol{\rho}} \hat{\psi}_{l_3}(\boldsymbol{\rho}) \cdot \nabla_{\boldsymbol{\rho}} \hat{\psi}_{l_4}(\boldsymbol{\rho}) d\boldsymbol{\rho} + \text{H.c.}, \tag{S23}$$

with selection rules $\delta_{l_2+l_3,l_4}$, $\delta_{l_2+l_4,l_3}$, $\delta_{l_3+l_4,l_2}$, and $\delta_{l_2+l_3+l_4,0}$. The processes in Eqs. (S22) and (S23) describe the confluence of two low-energy magnons into a single one and *vice versa*, with an efficiency determined by the coherent-magnon amplitude.

In the lowest band, $H_{\rm int}^{(1)}$ vanishes because $\mathcal{U}_{0000} = 0$. Energy-conserving scattering processes in

$$\begin{aligned}\hat{H}_{\rm int}^{(2)} &\to 2V_0 \Xi^*(t) \int \hat{\psi}_0^\dagger(\boldsymbol{\rho}) \nabla_{\boldsymbol{\rho}} \hat{\psi}_0(\boldsymbol{\rho}) \cdot \nabla_{\boldsymbol{\rho}} \hat{\psi}_0(\boldsymbol{\rho}) d\boldsymbol{\rho} + \text{H.c.}\\ &= -2V_0 \Xi^*(t) \sum_{\mathbf{kq}} (\mathbf{k}-\mathbf{q})\cdot\mathbf{q}\, \hat{\psi}_{0,\mathbf{k}}^\dagger \hat{\psi}_{0,\mathbf{k}-\mathbf{q}} \hat{\psi}_{0,\mathbf{q}} + \text{H.c.}\end{aligned} \tag{S24}$$

require that $k^2 \approx |\mathbf{k}-\mathbf{q}|^2 + q^2$ or $(\mathbf{k}-\mathbf{q})\cdot\mathbf{q} \approx 0$. We therefore may disregard interaction effects within the lowest band and focus on the interband scatterings.

Most intriguing is the up-conversion of two magnons into nearly empty states, creating a hot magnon out of two cold ones. The leading order scattering processes conserve energy:

$$\left(\frac{l_3\pi}{s}\right)^2 + \left(\frac{l_4\pi}{s}\right)^2 + (\mathbf{k}-\mathbf{q})^2 + q^2 \approx \left(\frac{l_2\pi}{s}\right)^2 + k^2, \tag{S25}$$

so

$$(\mathbf{k}-\mathbf{q})\cdot\mathbf{q} \approx \frac{l_3^2 + l_4^2 - l_2^2}{2}\frac{\pi^2}{s^2}. \tag{S26}$$

The interaction Hamiltonian then reduces to

$$\hat{H}_{\rm int} = \sum_{l_2 l_3 l_4} \sum_{\mathbf{k},\mathbf{q}} \mathcal{W}_{l_2 l_3 l_4} \Xi^*(t) \hat{\psi}_{l_2,\mathbf{k}}^\dagger \hat{\psi}_{l_3,\mathbf{k}-\mathbf{q}} \hat{\psi}_{l_4,\mathbf{q}} + \text{H.c.}, \tag{S27}$$

where

$$\begin{aligned}\mathcal{W}_{l_2 l_3 l_4} &= 2\left[\mathcal{U}_{0 l_2 l_3 l_4} - V_{0 l_2 l_3 l_4}(\mathbf{k}-\mathbf{q})\cdot\mathbf{q}\right]\\ &\approx 2\left(\mathcal{U}_{0 l_2 l_3 l_4} + \mathcal{V}_{0 l_2 l_3 l_4}\frac{l_2^2 - l_3^2 - l_4^2}{2}\frac{\pi^2}{s^2}\right)\end{aligned} \tag{S28}$$

is a contact potential since it does not depend on the wave number. Because of the selection rules $\delta_{l_2+l_3,l_4}$, $\delta_{l_2+l_4,l_3}$, and $\delta_{l_3+l_4,l_2}$, the scattering potential vanishes by a cancellation of the $\mathcal{U}$ and $\mathcal{V}$ terms: when $l_4 = l_2+l_3$ and $l_3 = l_2 + l_4$, $(l_2^2 - l_3^2 - l_4^2)/2 = -l_3 l_4$ while when $l_2 = l_3 + l_4$, $(l_2^2 - l_3^2 - l_4^2)/2 = l_3 l_4$. In conclusion, the coherent magnon amplitude in the lowest subbands interacts only with coherent magnons in the other subbands within the leading nonlinearity. We therefore may use a mean-field approximation to describe the dynamics of low-energy coherent magnons in the nonlinear regime.

III. PARAMETER-DEPENDENCE OF SPIN CURRENTS AND SPIN-ORBIT INTERACTION

Here we discuss the maximal spin current excited by stripline microwaves as a function of material parameters. For small stripline currents $I < I_c$, the coherently excited spin currents shown in Fig. S1 turns out to be proportional to I, rather thant I^2 as expected for non-interacting magnons. We oberve saturation at a critical drive I_c, and suppression for $I > I_c$ by high-order magnon interactions that are implicitly included in the numerical solutions of the LLG equation. The maximum spin current $\mathbf{J}_y^{(c)} \approx 10^{-7}$ kg/(m.s) is smaller but always close to that required for the Doppler-shift–induced spin-wave instability calculated by our mean-field theory, which turns out to be a good estimate for the maximal spin current.

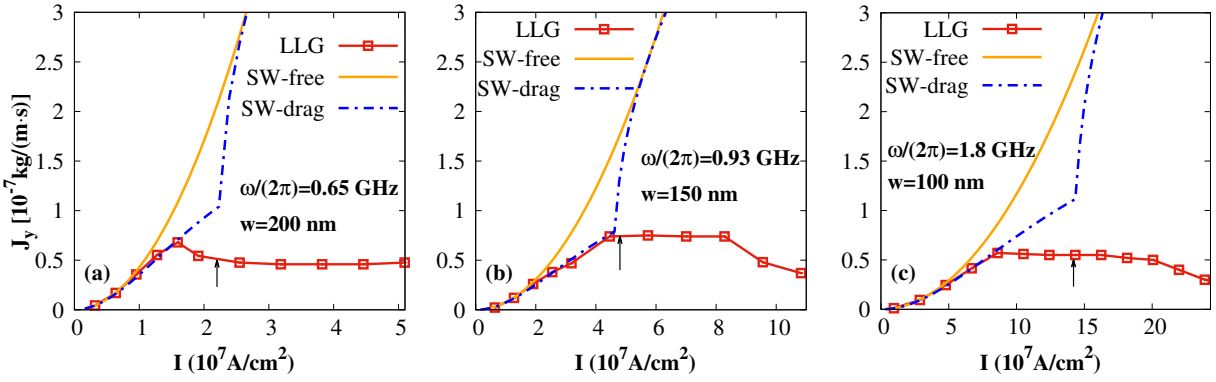

FIG. S1. Coherently pumped magnon current $\mathbf{J}_y$ as a function of the applied electric current density I in the stripline from numerical LLG calculations ("LLG"), non-interacting spin-wave theory ("SW-free"), and spin-wave theory including the drag effect ("SW-drag"). The black arrows indicate the critical current I_c that causes a spin-wave instability in the mean-field theory.

In the presence of an interfacial Dzyaloshinskii-Moriya spin-orbit interaction [1]

$$\hat{H}_{\rm DMI} = -\frac{D}{2\mu_0 M_s^2}\int d\mathbf{r}\left[\hat{\mathbf{y}}\cdot(\mathbf{M}\times\partial_z\mathbf{M}) - \hat{\mathbf{z}}\cdot(\mathbf{M}\times\partial_y\mathbf{M})\right], \tag{S29}$$

where D is the DMI constant, the magnon dispersion [Eq. (11) in the main text] to leading order reads

$$\omega_{k_y} = \mu_0\gamma H_{\rm app} + \omega_M\alpha_{\rm ex}k_y^2 - [\gamma D/M_s + (8/\hbar^2)\mathcal{V}_0 k_y \overline{\mathbf{J}}_y]k_y. \tag{S30}$$

Figure S2 illustrates that a $D = 7.5\times10^{-5}$ J/m^2 reduces the critical spin current to a value $\overline{\mathbf{J}}_y^{(c)} \approx 0.5\times10^{-7}$ kg/(m s) that according to the LLG equation augmented by the effective magnetic field from Eq. (S29), can be excited by a stripline. A sufficiently large spin-orbit interaction can therefore assist the generation of a Doppler-shift–induced spin-wave instability of the ground state magnetization.

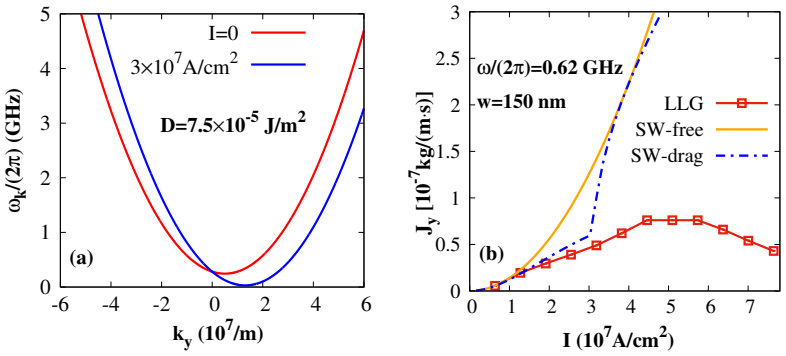

FIG. S2. Magnon dispersion [(a)] and coherently pumped spin current density $\mathbf{J}_y$ as a function of the applied electric current density I in the stripline [(b)] in the presence of a DMI spin-orbit interaction. The curves in (b) are obtained by numerically solving the LLG equation ("LLG"), by non-interacting spin-wave theory ("SW-free"), and by spin-wave theory including the drag effect ("SW-drag").

[1] J.-H. Moon, S.-M. Seo, K.-J. Lee, K.-W. Kim, J. Ryu, H.-W. Lee, R. D. McMichael, and M. D. Stiles, Phys. Rev. B **88**, 184404 (2013).